Recent work on the evolution of the global climate during the Cenozoic era has focused almost exclusively on the possible perturbation of atmospheric CO_2 levels resulting from weathering of silicates, especially in the Himalaya[5,6,29,30]. But Himalayan erosion produces very large C_{org} fluxes[20,31,32]. Although the hypothesized link between Himalayan silicate weathering and atmospheric CO_2 levels remains poorly quantified, our results indicate that increased sedimentary C_{org} storage resulting from Neogene Himalayan erosion and weathering has had a significantly larger effect on the carbon cycle than silicate weathering, by a factor of 2–3. Both models of the net change in the global sedimentary Corg reservoir[7,26] and data from the Himalayan–Bengal system are consistent with the hypothesis that an excess of C_{org} burial over weathering acted as a sink for atmospheric CO_2 during the Neogene. □

Received 13 February; accepted 18 August 1997.

1. Garrels, R. M. & Perry, E. A. Cycling of carbon sulfur and oxygen through geologic time. in *The Sea* 303–336 (1974).
2. Lasaga, A. C., Berner, R. A. & Garrels, R. M. in *The Carbon Cycle and Atmospheric CO_2: Natural Variations, Archean to Present* (eds Sundquist, E. T. & Broecker, W. S.) 397–410 (American Geophysical Union, Washington DC, 1985).
3. Berner, R. A. Atmospheric CO_2 levels over Phanerozoic time. *Science* **249,** 1382–1386 (1990).
4. Walker, J. C. G., Hays, P. B. & Kasting, J. F. A negative feed back mechanism for the long-term stabilization of Earth's surface temperature. *J. Geophys. Res.* **86,** 9776–9782 (1981).
5. Raymo, M. E. & Ruddiman, W. F. Tectonic forcing of late Cenozoic climate. *Nature* **359,** 117–122 (1992).
6. Molnar, P., England, P. & Martinod, J. Mantle dynamics, uplift of the Tibetan Plateau, and the Indian monsoon. *Rev. Geophys.* **31,** 327–396 (1993).
7. Goddéris, Y. & François, L. M. Balancing the Cenozoic carbon and alkalinity cycles: Constraints from isotopic records. *Geophys. Res. Lett.* **23,** 3743–3746 (1996).
8. Einsele, G., Ratschbacher, L. & Wetzel, A. The Himalaya–Bengal fan denudation accumulation system during the past 20 Ma. *J. Geol.* **104,** 163–184 (1996).
9. France-Lanord, C., Derry, L. & Michard, A. in *Himalayan Tectonics* (eds Treloar, P. J. & Searle, M.) 603–621 (Geol. Soc. Lond., London, 1993).
10. Sayles, F. L. & Mangelsdorf, P. C. The equilibration of clay minerals with seawater: exchange reactions. *Geochim. Cosmochim. Acta* **41,** 951–960 (1977).
11. Von Damm, K. L., Edmond, J. M., Grant, B. & Measures, C. K. Chemistry of submarine hydrothermal solutions at 21° N, East Pacific Rise. *Geochim. Cosmochim. Acta* **49,** 2197–2220 (1985).
12. France-Lanord, C. Chevauchement, métamorphisme et magmatisme en Himalaya du Népal central. Etude isotopique H, C, O. Thesis, Institut National Polytechnique de Lorraine (1987).
13. Beck, R. A., Burbank, D. W., Sercombe, W. J., Olson, T. L. & Khan, A. M. Organic carbon exhumation and global warming during the early Himalayan collision. *Geology* **23,** 387–390 (1995).
14. Shipboard Scientific Party. Initial Reports Sites 717-718-719 Distal Bengal Fan, *Proc. ODP Init. Rep.* (Ocean Drilling Program, College Station, TX, 1989).
15. Bouquillon, A., France-Lanord, C., Michard, A. & Tiercelin, J.-J. in *Proc. ODP Sci. Res.* (eds Cochran, J. R. *et al.*) 43–58 (1990).
16. Derry, L. A. & France-Lanord, C. Neogene Himalayan weathering history and river $^{87}Sr/^{86}Sr$: Impact on the marine Sr record. *Earth Planet. Sci. Lett.* **142,** 59–74 (1996).
17. Martin, J. M. & Meybeck, M. Element mass-balance of material carried by major world rivers. *Mar. Chem.* **7,** 173–206 (1979).
18. Sarin, M. M., Krishnaswami, S., Dilli, K., Omayajulu, B. l. K. & Moore, W. S. Major ion chemistry of the Ganga–Brahmaputra river system: Weathering processes and fluxes to the Bay of Bengal. *Geochim. Cosmochim. Acta* **53,** 997–1009 (1989).
19. Gardner, R. & Walsh, N. Chemical weathering oif metamorphic rocks from low elevations in the southern Himalaya. *Chem. Geol.* **127,** 161–176 (1996).
20. France-Lanord, C. & Derry, L. A. $\delta^{13}C$ or organic carbon in the Bengal fan: source evolution and transport of C3 and C4 plant carbon to marine sediments. *Geochim. Cosmochim. Acta* **58,** 4809–4814 (1994).
21. Bouquillon, A. *Influence continentale et marine dans les sediments Cénozoiques de l'océan Indien Nord Oriental.* Thesis, Université de Lille Flandres-Artois (1987).
22. Berner, R. A. & Berner, E. *Global Environment: Water, Air, and Geochemical Cycles* 1–376 (Prentice Hall, Upper Saddle River, NJ, 1994).
23. Michalopoulos, P. & Aller, R. C. Rapid clay mineral formation in Amazon delta sediments: Reverse weathering and oceanic elemental cycles. *Science* **270,** 614–617 (1995).
24. Milliman, J. D. & Syvitski, P. M. Geomorphic/tectonic control of sediment discharge ot the ocean: the importance of small mountainous rivers. *J. Geol.* **100,** 525–544 (1992).
25. Shackleton, S. J. & Hall, M. A. Carbon isotope data from Leg 74 sediments. in *Init. Rep. DSDP* (eds Moore, T. C. *et al.*) 613–619 (US Govt Printing Office, Washington, 1984).
26. Derry, L. A. & France-Lanord, C. Neogene growth of the sedimentary organic carbon reservoir. *Paleoceanography* **11,** 267–275 (1996).
27. Berner, R. A. & Canfield, D. A model for atmospheric oxygen over Phanerozoic time. *Am. J. Sci.* **289,** 333–361 (1989).
28. Hedges, J. I. & Keil, R. G. Sedimentary organic matter preservation: an assessment and speculative synthesis. *Mar. Chem.* **49,** 81–90 (1995).
29. Raymo, M. E. The Himalayas, organic carbon burial, and climate in the Miocene. *Paleoceanography* **9,** 399–404 (1994).
30. Caldeira, K. Enhanced Cenozoic chemical weathering and the subduction of pelagic carbonate. *Nature* **357,** 578–581 (1992).
31. Subramanian, V. & Ittekkot, V. Carbon transport by the Himalayan rivers. in *Biogeochemistry of Major World Rivers, SCOPE* (eds Degens, E. T., Kempe, S. & Richey, J. E.) 157–168 (Wiley, Chichester, 1991).
32. Ittekkot, V. Global trends in the nature of organic matter in river suspensions. *Nature* **332,** 436–438 (1988).

Acknowledgements. We thank Patrick Le Fort for providing part of the Himalayan samples and analyses. This study was supported by the CNRS-INSU program 'Dynamique et Bilan de la Terre-Fleuve et Érosion'.

Correspondence should be addressed to C.F.-L. at CRPG-CNRS (e-mail: cfl@crpg.cnrs-nancy.fr).

Mechanical power output of bird flight

K. P. Dial*, A. A. Biewener†, B. W. Tobalske* & D. R. Warrick*

** Division of Biological Sciences, University of Montana, Missoula, Montana 59812, USA*
† Department of Organismal Biology and Anatomy, University of Chicago, 1025 East 57 Street, Chicago, Illinois 60637, USA

Aerodynamic theory predicts that the power required for an animal to fly over a range of speeds is represented by a 'U'-shaped curve, with the greatest power required at the slowest and fastest speeds, and minimum power at an intermediate speed[1–6]. Tests of these predictions, based on oxygen consumption measurements of metabolic power in birds[7–12] and insects[13], support a different interpretation, generating either flat or 'J'-shaped power profiles, implying little additional demand between hovering and intermediate flight speeds[14]. However, respirometric techniques represent only an indirect assessment of the mechanical power requirements of flight and no previous avian study has investigated an animal's full range of attainable level flight speeds. Here we present data from *in vivo* bone-strain measurements of

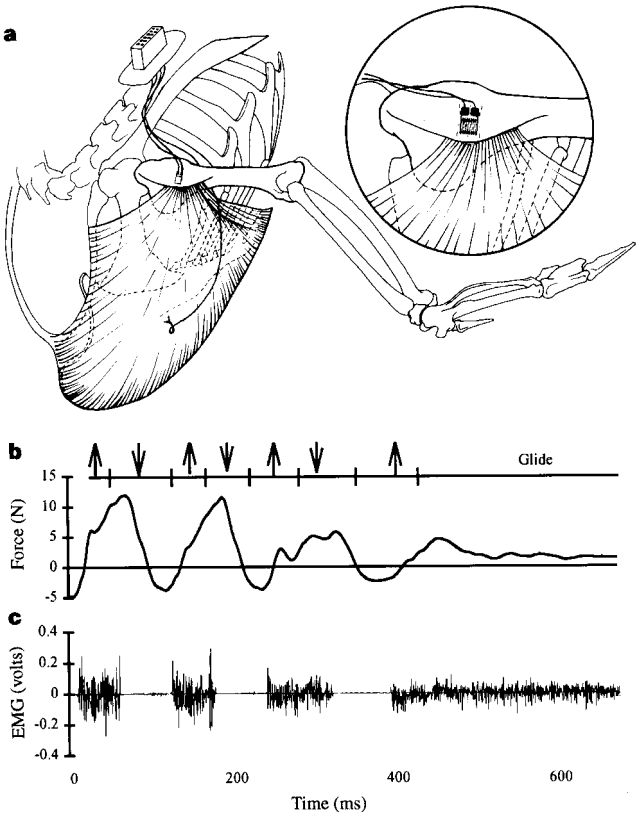

Figure 1 a, Illustration of a magpie pectoral girdle and forelimb showing the placement of a strain gauge on the delto-pectoral crest (DPC; expanded in inset) and indwelling bipolar electromyographic (EMG) wires in the pectoralis muscle, all connected to a dorsal plug. **b**, Recordings of DPC strain calibrated to pectoralis force (arrows indicate kinematic upstroke and downstroke) and **c**, corresponding pectoralis (EMG) for three successive wingbeats of a magpie flying at 6 m s^{-1}, were synchronized to wing kinematics (obtained from 16 mm high-speed movie film at 150–200 f.p.s. in lateral and dorsal views) to estimate pectoralis fibre length change in relation to force development and to determine wingbeat cycle duration.

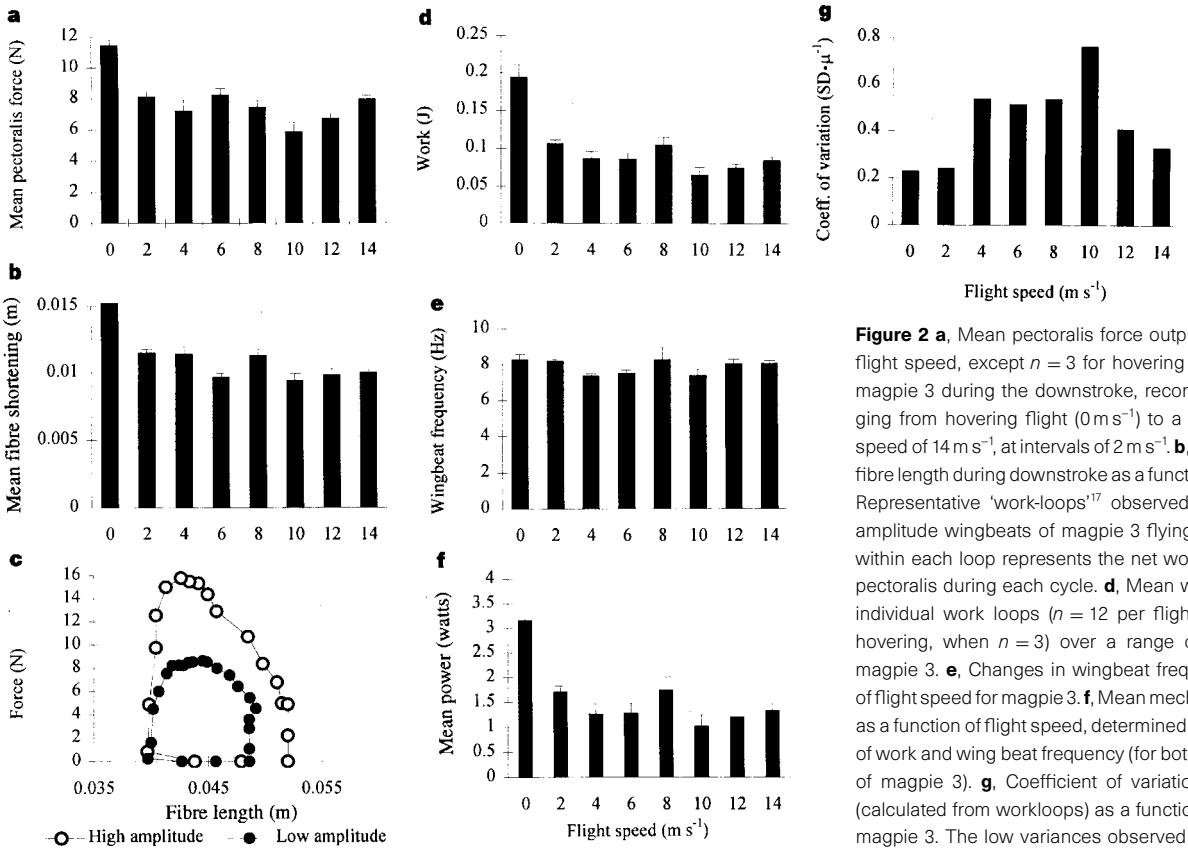

Figure 2 a, Mean pectoralis force output (±s.e.; $n = 12$ per flight speed, except $n = 3$ for hovering flight) generated by magpie 3 during the downstroke, recorded for speeds ranging from hovering flight (0 m s^{-1}) to a maximum observed speed of 14 m s^{-1}, at intervals of 2 m s^{-1}. **b**, Changes in muscle-fibre length during downstroke as a function of flight speed. **c**, Representative 'work-loops'[17] observed for high- and low-amplitude wingbeats of magpie 3 flying at 6 m s^{-1}; the area within each loop represents the net work performed by the pectoralis during each cycle. **d**, Mean work calculated from individual work loops ($n = 12$ per flight speed, except for hovering, when $n = 3$) over a range of flight speeds for magpie 3. **e**, Changes in wingbeat frequency as a function of flight speed for magpie 3. **f**, Mean mechanical power output as a function of flight speed, determined from measurements of work and wing beat frequency (for both pectoralis muscles of magpie 3). **g**, Coefficient of variation for power output (calculated from workloops) as a function of flight speed for magpie 3. The low variances observed at hovering and the highest flight speeds suggest that the bird was performing at or near to its performance limit. Comparable data to those shown here were obtained for the other two magpies.

pectoralis muscle force coupled with wing kinematics in black-billed magpies (*Pica pica*), which we use to calculate mechanical power directly. As these birds flew over their full range of speeds, we offer a complete profile of mechanical power output during level flapping flight for this species. Values of mechanical power output are statistically indistinguishable (that is, the power curve is flat) over most forward-flight speeds but are significantly higher during hovering and flight at very low speeds.

We flew birds in a variable-speed wind tunnel[15,16] to measure the force generated by the dominant flight muscles by means of bone-strain recordings (Figs 1, 2a) and to determine muscle-fibre shortening from analysis of wing excursion (Fig. 2b). Changes in force plotted against changes in fibre length (Fig. 2c) show the net total work (area of 'work loop')[17] of the pectoralis during a wingbeat cycle. By combining measurements of work per cycle (Fig. 2d) with wingbeat frequency (Fig. 2e), we calculated the mechanical power generated by the pectoralis muscles over a range of steady flight speeds. The results obtained from our measurements and analyses show that the mechanical power output (mean body-mass-specific power) is maximal during hovering (~21 W kg^{-1} at 0 m s^{-1}), decreases markedly with an increase in forward speed (~9 W kg^{-1} at 4 m s^{-1}), remains relatively constant over a broad range of faster flight speeds (4 to 12 m s^{-1}), and increases slightly during the maximum flight speed measured (~12 W kg^{-1} at 14 m s^{-1}) (Figs 2, 3). This pattern is borne out by the generally uniform measurements of force, fibre shortening and wingbeat frequency (Fig. 2a, b, e) that we observed over the intermediate speed range, and the maximum pectoralis force generation and fibre shortening during hovering. Correspondingly, the low values in the coefficients of variation (CV) of power output at the lowest and highest flight speeds, and the more or less stereotypic wingbeat excursions, suggest that each animal was performing at or near its limit at these speeds (Fig. 2g). In contrast, higher CV values at intermediate flight speeds reflect the use of variable wing excursions[18], which resulted in constant power production over a wide range of flight speeds. We propose that alterations in wing and tail configuration during different flight speeds account for the differences in mechanical power otherwise predicted by quasi steady-state aerodynamic theory of vertebrate flight.

Our calculations of mechanical power output are consistent with estimates from previous metabolic studies[8–12] at intermediate speeds. However, as previous metabolic data do not describe the energetic cost of flight over each species' full range of speeds (that is, from hovering to maximum flapping flight), the power profiles are incomplete (Fig. 3b). This is undoubtedly due to the difficulty (or impossibility) of obtaining reliable steady-state measurements of oxygen consumption during extremely slow flight speeds (0–4 m s^{-1}). In contrast, the technique we describe provides instantaneous (that is, per wingbeat) measurements of muscle mechanical power during hovering and very slow flight.

Our measurements show that power output is maximal during hovering. Comparable levels of power output are not observed at the upper range of flying speeds. As hovering episodes are brief (1–4 s), we suggest that non-forward flapping flight in this species, as in other species, may involve anaerobic metabolism within the pectoralis. Similarly, sustainable flight at speeds greater than 14 m s^{-1} may not be possible because anaerobic metabolism cannot be sustained. Thus, the 'shape' of the power curve will be determined by the particular species' available aerobic power. Birds that can sustain higher levels of mass-specific power output may be more likely to fly at very slow and fast speeds, exhibiting high induced power (slow) or high profile and parasite power (fast)[14].

We suggest that the 'L'-shaped power profile exhibited by magpies reflects the power required for birds of similar wing design and body

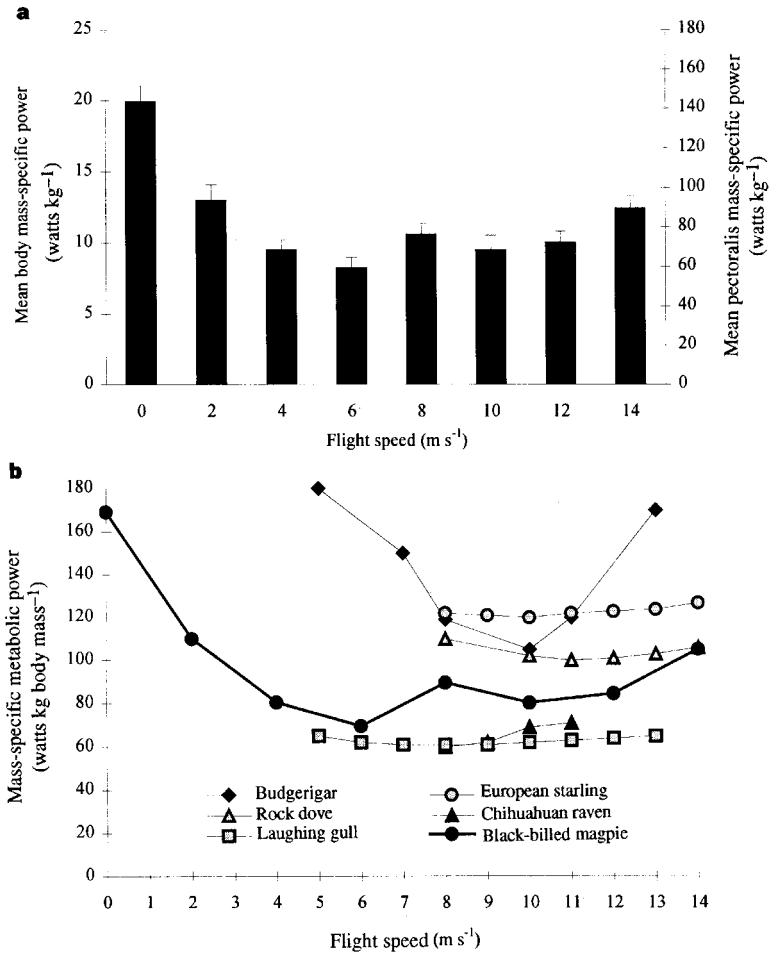

Figure 3 a, Summary of the mean total mechanical power output measured for all three magpies as a function of flight speed. Whereas power output during hovering was significantly higher ($P < 0.001$) than at all other speeds, no significant differences in power were observed between 4 and 14 m s^{-1}. Probability values were derived from repeated measures ANOVA with post-hoc comparison of power output versus speed ($n = 3$ or 10 wingbeats per flight speed). **b**, Comparison of our present data for mechanical power output of the magpie (bold line) with mass-specific metabolic power output data previously reported for various bird species[6], based on a muscle efficiency of 11.75%. This value was obtained by averaging the results obtained for the metabolic[11,12] and mechanical power[15,18] output of starlings (13.0% at 11–14 m s^{-1}) and pigeons (10.5% at 7–9 m s^{-1}) during forward flight. All bird studies[8–12], with the exception of the budgerigar[7], show power output during level flapping flight to be relatively flat (that is, constant) over most speeds recorded. Note that at low flight speeds (0 and 2 m s^{-1}), birds clearly recruit many additional muscles (such as tail and antebrachial muscles) that do no measurable mechanical work[25], so our technique may underestimate the metabolic power required at these speeds.

mass. However, the flight of other species of birds may not adhere to the 'L'-shaped power curve that we describe for magpies. Hummingbirds, for example, have a unique shoulder arrangement that permits a wing movement to generate lift during both 'upstroke' and 'downstroke', perhaps allowing members of this group to hover using significantly less mass-specific mechanical power output than other small birds[5,14,19]. Testing the generality of the profile of mechanical power output for magpies requires that similar measurements be made for a number of avian species having disparate wing structure. The fact that birds do not appear to adhere to a strict 'U'-shaped power curve may help to explain why field observations[20,21] frequently fail to agree with the theoretically predicted[4] minimum power and maximum range flight velocities. Such theories do not adequately account for the ability of birds to dramatically change wing and tail presentation over a range of flight speeds[18], permitting these animals to alter significantly the power requirements for flight. □

Methods

Animals and strain measurements. Following training to fly in a variable-speed wind tunnel[16,18] over nearly their full range of flight speeds (hovering to 14 m s^{-1}), *in vivo* measurements of pectoralis muscle force were obtained from three black-billed magpies (mean mass, 174 g), based on bone-strain recordings made at the dorsal surface of the deltopectoral crest (DPC)[15,22]. The DPC serves as the insertion site for the pectoralis on the proximo–anterior surface of the humerus and as such the DPC's dorsal surface experiences tensile strains as the pectoralis develops force. Our measurements assume that the power generated by the pectoralis muscles approximates the total mechanical power of the bird during flight[23,24]. However, this method may slightly underestimate the mechanical power requirements during very slow or hovering flight as it ignores the inertial power generated by the supracoracoideus and/or other upstroke muscles[25]. The strain gauge was attached perpendicularly to the bone's shaft to avoid sensitivity to strains produced by bending and torsional loading of the humerus and associated with aerodynamic loading of the wing[19]. Following recovery from strain gauge and electrode implantation, birds were flown at speeds from 0 to 14 m s^{-1} at 2 m s^{-1} intervals. Birds were flown first at an intermediate speed, with subsequent speed trials conducted in a random order. DPC strains were then calibrated *in situ* in fully anaesthetized animals, using a force transducer attached to the pectoralis muscle by a heavy nylon thread tied around the muscle's aponeurotic insertion below the ventral surface of the DPC, so that cyclic forces could be applied in the direction of the muscle's pull during flight. Force calibrations were made with the wings held at 60°, 30° and horizontal in order to obtain a mean calibration. After calibration, the strain gauge and electromyogram electrodes were removed and the birds allowed to recover.

Measurements of muscle fibre length. Changes in muscle fibre length as a function of flight speed were estimated from measurements of wingbeat amplitude by digitizing wingtip elevation (h) and wing length from lateral and dorsal views of high-speed film to calculate the wing excursion angle, $\theta = \sin^{-1}(h/b)$, where b is the extended wing length at mid-downstroke. Pectoralis fibre length change (Δl) was then calculated as the arc of movement of the humerus at the DPC ($\Delta l = \Delta\theta r$), based on the measurements of wing excursion angle and the muscle's moment arm (r) at the shoulder. This method assumes that excursions of the wing and humerus are uniformly maintained with respect to one another over the animal's entire flight speed range. Relative changes in pectoralis fibre-length change were then calculated on the basis of the measurement of an average resting fibre length made directly from the pectoralis of one of the magpies used in the wind-tunnel trials.

Calculating work loops. Changes in force plotted against changes in fibre length provide the net total work of the pectoralis during a wingbeat cycle. Multiplying measurements of work per cycle by wingbeat frequency yields mechanical power generated by the muscles.

Received 11 June; accepted 11 August 1997.

1. Tucker, V. A. Bird metabolism during flight: evaluation of a theory. *J. Exp. Biol.* **58,** 689–709 (1973).
2. Pennycuick, C. J. Power requirements for horizontal flight in the pigeon *Columba livia*. *J. Exp. Biol.* **49,** 527–555 (1968).
3. Pennycuick, C. J. in *Avian Biology* (eds. Farner, D. S. & King, J. R.) **5,** 1–75 (1975).
4. Pennycuick, C. J. *Bird Flight Performance* (Univ. Press, Oxford, 1989).
5. Rayner, J. M. V. A new approach to animal flight mechanics. *J. Exp. Biol.* **80,** 17–54 (1979).
6. Norberg, U. M. *Vertebrate Flight* (Springer, Berlin, 1990).
7. Tucker, V. A. Respiratory exchange and evaporative water loss in the flying budgerigar. *J. Exp. Biol.* **48,** 67–87 (1968).
8. Tucker, V. A. Metabolism during flight in the laughing gull, *Larus atricilla*. *Am. J. Physiol.* **222,** 237–245 (1972).
9. Hudson, D. M. & Bernstein, M. H. Gas exchange and energy cost of flight in the white-necked raven, *Corvus cryptoleucus*. *J. Exp. Biol.* **103,** 121–130 (1983).
10. Berger, M., Hart, O. Z. & Roy, J. S. Respiration, oxygen consumption and heart rate in some birds during rest and flight. *Z. Vergl. Physiol.* **66,** 201–214 (1970).
11. Torre-Bueno, J. R. & LaRochelle, J. The metabolic cost of flight in unrestrained birds. *J. Exp. Biol.* **75,** 223–229 (1978).
12. Rothe, H.-J., Biesel, W. & Nachtigall, W. Pigeon flight in a wind tunnel. II. Gas exchange and power requirements. *J. Comp. Physiol. B* **157,** 99–109 (1987).
13. Ellington, C. P., Machin, K. I. & Casey, T. M. Oxygen consumption of bumblebees in forward flight. *Nature* **347,** 472–473 (1990).
14. Ellington, C. P. Limitations on animal flight performance. *J. Exp. Biol.* **160,** 71–91 (1991).
15. Dial, K. P. & Biewener, A. A. Pectoralis muscle force and power output during different modes of flight in pigeons (*Columba livia*). *J. Exp. Biol.* **176,** 31–54 (1993).
16. Tobalske, B. W. & Dial, K. P. Neuromuscular control and kinematics of intermittent flight in budgerigars (*Melopsittacus undulatus*). *J. Exp. Biol.* **187,** 1–13 (1994).
17. Josephson, R. K. The mechanical power output of a tettigonid wing muscle during singing and flight. *J. Exp. Biol.* **117,** 357–368 (1985).
18. Tobalske, B. W. & Dial, K. P. Flight kinematics of black-billed magpies and pigeons over a wide range of speeds. *J. Exp. Biol.* **199,** 263–280 (1996).
19. Biewener, A. A. & Dial, K. P. *In vivo* strain in the pigeon humerus during flight. *J. Morph.* **225,** 61–75 (1995).
20. Hedenstrom, A. & T. Alerstam. Skylark optimal flight speeds for flying nowhere and somewhere. *Behav. Ecology* **7,** 121–126.
21. Liechti, F., Ehrich, D. & Bruderer, B. Flight behaviour of white storks *Ciconia ciconia* on their migration over Southern Israel. *Ardea* **84,** 3–13 (1997).
22. Biewener, A. A., Dial, K. P. & Goslow, G. E. Jr Pectoralis muscle force and power output during flight in the starling. *J. Exp. Biol.* **164,** 1–18 (1992).
23. Dial, K. P. Activity patterns of the wing muscles in the pigeon (*Columba livia*) during different modes of flight. *J. Exp. Zool.* **262,** 357–373 (1992).
24. Dial, K. P. Avian forelimb muscles and nonsteady flight: can birds fly without using the muscles in their wings? *Auk* **109,** 874–885 (1992).
25. Van Den Berg, C. & Rayner, J. M. V. The moment of inertia of bird wings and the inertial power requirement for flapping flight. *J. exp. Biol.* **198,** 1655–1664 (1995).
26. Scholey, K. D. Evelopments in Vertebrate Flight: Climbing and Gliding of Mammals and Reptiles and the Flapping Flight of Birds. thesis, Univ. Bristol (1983).

Acknowledgements. We thank F. A. Jenkins Jr for his thoughtful input on previous drafts of this manuscript; M. LaBarbera, J. M. Marzluff, D. Fawcett and D. F. Boggs for their comments; and J. Gilpin for making the force-transducer used to calibrate the DPC strain recordings. Supported by grants from the NSF to K.P.D. and A.A.B.

Correspondence and requests for materials should be addressed to K.P.D. (e-mail: kdial@selway.umt.edu).

Impaired odour discrimination on desynchronization of odour-encoding neural assemblies

Mark Stopfer*, Seetha Bhagavan†‡, Brian H. Smith† & Gilles Laurent*

* *California Institute of Technology, Biology Division, 139-74, Pasadena, California 91125, USA*

† *Ohio State University, Department of Entomology, 1735 Neil Avenue, Columbus, Ohio 4210-1220, USA*

Stimulus-evoked oscillatory synchronization of neural assemblies has been described in the olfactory[1–5] and visual[6–8] systems of several vertebrates and invertebrates. In locusts, information about odour identity is contained in the timing of action potentials in an oscillatory population response[9–11], suggesting that oscillations may reflect a common reference for messages encoded in time. Although the stimulus-evoked oscillatory phenomenon is reliable, its roles in sensation, perception, memory formation and pattern recognition remain to be demonstrated—a task requiring a behavioural paradigm. Using honeybees, we now demonstrate that odour encoding involves, as it does in locusts, the oscillatory synchronization of assemblies of projection neurons and that this synchronization is also selectively abolished by picrotoxin, an antagonist of the $GABA_A$ (γ-aminobutyric acid) receptor. By using a behavioural learning paradigm, we show that picrotoxin-induced desynchronization impairs the discrimination of molecularly similar odorants, but not that of dissimilar odorants. It appears, therefore, that oscillatory synchronization of neuronal assemblies is functionally relevant, and essential for fine sensory discrimination. This suggests that oscillatory synchronization and the kind of temporal encoding it affords provide an additional dimension by which the brain could segment spatially overlapping stimulus representations.

Investigation of olfactory processing in the locust antennal lobe—a functional and morphological analogue of the vertebrate olfactory bulb—has indicated that both monomolecular and complex odours are represented there combinatorially by dynamical assemblies of projection neurons[5,9–11]. Each neuron in an odour-coding assembly responds with an odour-specific temporal firing pattern consisting of periods of activity and silence[5,9]. Any two neurons responding to the same odour are usually co-active only during a fraction of the population response. The spikes of co-activated neurons are generally synchronized[5,9,10] by the distributed action of GABA-ergic local neurons[12], resulting in large-amplitude, 20–35 Hz local field potential (LFP) oscillations in their target area, the calyx of the mushroom body[5]. Each successive cycle of the odour-evoked oscillatory LFP can therefore be characterized by a co-active subset of projection neurons, and an odour is thus represented by a specific succession of synchronized assemblies[10,11]. This representation thus comprises three main features—the identity of the odour-activated neurons, the temporal evolution of the ensemble, and oscillatory synchronization—whose importance to the animal for learning and recognition needs to be examined.

We have previously shown that picrotoxin (PCT) applied to the locust antennal lobe selectively blocks the fast inhibitory synapse between local and projection neurons and abolishes their oscillatory synchronization: this manipulation altered neither the response profiles of projection neurons to odours, nor their odour specificity[12]. We have now made use of this pharmacological tool to assess whether oscillatory synchronization plays a role in odour learning and discrimination, an experiment that requires a behavioural assay. We therefore used honeybees, which can be trained to extend their mouth parts (proboscis) in response to specific odours after a few associative forward pairings of these odours with a sucrose reinforcement (proboscis-extension (PE) conditioning)[13–15]. First, we demonstrated that odour representation in the honeybee includes the same three features as those discovered in the locust; second, we tested the importance of oscillatory synchronization for odour learning and discrimination.

Odours, but not air alone, puffed onto an antenna of a honeybee evoked bouts of ~30 Hz LFP oscillations in the calyx of the ipsilateral mushroom body (for example, mint; Fig. 1a). These oscillations lasted for ~0.5–1 s in response to a 1-s long odour puff. Sliding-window autocorrelations of these LFPs revealed the sustained periodic structure of the odour-evoked responses (Fig. 1a). Simultaneous intracellular recordings from antennal lobe neurons showed that, as in locusts[5], individual antennal lobe neurons responded selectively to certain odours with prominent membrane-potential oscillations (Figs 1b, 3a; $n = 21$ neurons in 16 animals) which are locked to the mushroom body LFP (Fig. 1c, d). Mushroom body LFP oscillations lagged behind those in antennal lobe neurons (phase, $-53° \pm 5$; mean ± s.e.m.; $n = 290$ cycles, where 0° is defined as the peak of the LFP; Fig. 1c). This is consistent with our findings in locusts, in which LFP oscillations in the mushroom body result, at least in part, from the coherent input

‡ Present address: GICCS, Research Building Room WP-18, Georgetown University Medical Center, 3970 Reservoir Rd, N.W. Washington, DC 20007-2197, USA.